Sensors and Materials, Vol. 38, No. 2 (2026) 775–784
MYU Tokyo

S & M 4347

Effects of Thermal Treatment on the Sensitivity of Polycrystalline Silicon Nanowire FET Biosensors

Yu-Liang Hsu,[1] Yuan-Nan Tsai,[2] Chu-En Lin,[2]
Nitthita Chirdchoo,[3] I-Nan Chang,[4] and Chi-Chang Wu[2*]

[1]Department of Mechanical and Electromechanical Engineering, National Sun Yat-sen University, Kaohsiung 804201, Taiwan
[2]Department of Electronic Engineering, National Chin-Yi University of Technology, Taichung 411030, Taiwan
[3]Department of Electrical Engineering, Nakhon Pathom Rajabhat University, Nakhon Pathom 73000, Thailand
4Department of Electronics Engineering, Feng Chia University, Taichung 40724, Taiwan

(Received April 30, 2025; accepted August 27, 2025)

Keywords: nanowire, nanowire FET, thermal treatment, pH sensing

In this study, we developed polycrystalline silicon (poly-Si) nanowires by a sidewall spacer technique and employed them to fabricate nanowire field-effect transistor (NWFET) devices for biomedical sensing applications. The impact of post-fabrication thermal treatments on the electrical performance of the poly-Si NWFET biosensors was systematically investigated. Among the tested conditions, the devices treated at 400 °C in vacuum exhibited significantly enhanced electrical characteristics. These optimized biosensors were then used for solution pH detection, demonstrating high sensitivity and a clear linear correlation between drain current and pH. Furthermore, real-time pH sensing experiments confirmed the biosensors' capability to respond rapidly and accurately to changes in pH, highlighting both their sensitivity and response speed. Overall, the developed poly-Si NWFET biosensors show strong potential for advancing medical diagnostics by enabling early disease detection and supporting personalized healthcare strategies.

1. Introduction

The rapid advancements in biotechnology are driving the development of next-generation medical devices, with *in vitro* diagnostic (IVD) devices being a central focus.[1,2] IVD devices are biomedical sensors designed to detect and diagnose diseases or symptoms through the analysis of body fluids or tissue samples, without direct contact with the human body.[3] These devices encompass reagents, sample collection tools, instruments, and systems that facilitate clinical diagnosis, disease monitoring, and prognosis. By analyzing biological markers, IVD devices enable physicians to make informed decisions regarding treatment plans and monitor disease progression. Additionally, they are instrumental in assessing disease risk and guiding preventive healthcare, potentially reducing future medical costs. IVD devices can be classified into several categories on the basis of their detection methods, including clinical biochemistry,

*Corresponding author: e-mail: ccwu@ncut.edu.tw
https://doi.org/10.18494/SAM5715

ISSN 0914-4935
https://myukk.org/

protein immunodiagnostics, molecular diagnostics, and hematology.[4,5] Key requirements for high-performance IVD devices include sensitivity, dynamic range, specificity, reproducibility, accuracy, and resistance to interference to ensure reliable diagnostic outcomes.[6]

Biomedical sensors play a crucial role in IVD devices. On the basis of sensing principles, biomedical sensors can be classified into four major types: mass sensing,[7] optical sensing,[8] electrochemical sensing,[9] and electric field sensing.[10–12] Among these methods, electric field sensing is particularly powerful, involving the placement of a component such as a FET in an electrolyte solution.[13] This configuration generates a surface potential at the gate sensing layer of the transistor.[14] Variations in ion concentration in the electrolyte alter the surface potential of the sensing layer, affecting the channel current flowing through the transistor. Notably, when the FET operates in the inversion region, even small changes in gate voltage can lead to exponential variations in drain current, effectively amplifying the sensing signal. Nanowire field-effect transistors (NWFETs) are well-established electric field sensing devices used for biomolecule monitoring.[15] In these devices, the nanowires are sensitive to charged molecules, resulting in variations in surface potential and the corresponding changes in drain current. This high sensitivity to minor fluctuations in molecular or ionic concentration enables NWFET sensors to deliver highly accurate and ultrasensitive detection, making them essential tools across a wide range of applications, from laboratory research to environmental monitoring and medical diagnostics.[16] Consequently, NWFET-based biosensors offer a significant advantage in amplifying weak signals, allowing for the precise detection of changes in biomolecule concentration across various sample matrices.

We have developed a polycrystalline silicon (poly-Si) NWFET device as a biosensor.[17] The fabrication cost of this poly-Si NWFET biosensor can be significantly reduced compared with those of their single-crystalline silicon counterparts while maintaining equivalent sensitivity. In this study, we aim to enhance the sensitivity of the poly-Si NWFET for biomolecule sensing, thereby contributing to the reduction of disease occurrences. Given that the surface characteristics of the poly-Si nanowires are critical to the performance of the NWFET biosensor, we investigated post-treatment conditions to improve the electrical performance and sensitivity of the biosensor.

Our results indicate that the biosensor's sensitivity can be further enhanced while ensuring stable performance over time. By identifying the optimal surface modification and operational conditions, the commercialization of this poly-Si NWFET biosensor becomes feasible, providing accessible and reliable biosensing solutions for disease prevention and diagnosis.

2. Materials and Methods

2.1 Nanowire FET device fabrication

The devices were fabricated on 6-inch p-type silicon wafers. A stacked film consisting of 1000 Å silicon dioxide (SiO_2) and 500 Å silicon nitride (Si_3N_4) was grown using a horizontal furnace system. This dielectric stack served both as an isolation layer and as the bottom-gate dielectric for the devices. Subsequently, a 1000 Å tetraethyl orthosilicate oxide layer was

deposited, followed by photolithography and dry etching to define a dummy gate structure. A 1000 Å amorphous silicon (α-Si) layer was then deposited over the wafer. α-Si nanowires were formed along the sidewalls of the dummy gate by a sidewall spacer etching technique, enabling self-aligned nanowire formation. These α-Si nanowires were then crystallized into poly-Si nanowires by post-annealing at 600 ℃ for 24 h. Following nanowire formation, standard source/drain implantation, passivation, and metallization steps were carried out, along with the remaining MOSFET fabrication processes, to complete the fabrication of poly-Si multi-gate NWFET devices.

2.2 Post-thermal treatments of biosensors

To improve the sensitivity of biosensors, post-fabrication thermal treatments were performed on the poly-Si NWFET devices. In this study, thermal annealing was conducted in vacuum or nitrogen (N_2) at various temperatures using a furnace. To clarify the experimental grouping, the samples are labeled according to their thermal treatment conditions as follows: 400Vac denotes samples annealed at 400 ℃ in vacuum, 200N2 indicates samples treated at 200 ℃ in nitrogen, 400N2 represents samples annealed at 400 ℃ in nitrogen, and control refers to samples without any post-fabrication thermal treatment; this unified nomenclature is consistently applied throughout all figures and discussions in the manuscript. Following the thermal treatments, the devices were passivated with a photoresist film and stored in N_2 atmosphere to preserve their stability before sensing.

2.3 Functionalization and bio-grafting of nanowire surface

To functionalize the sensor surface, an activation process was applied to the nanowires using oxygen plasma treatment. The devices were then immersed in an APTES/ethanol mixture for 30 min to introduce amino terminals onto the nanowire surface. After rinsing and heating to remove any unreacted residues, the NWFET devices were immersed in a diluted glutaraldehyde (GA) solution for 1 h. This step ensured that GA binds to the amino groups through its aldehyde functionality. Finally, the devices were rinsed with a bis-tris propane (BTP) solution and blow-dried using a nitrogen gun in preparation for biosensing.

3. Results and Discussion

Figure 1(a) shows an optical microscopy image of the formed poly-Si NWFET device. The SEM image of the fabricated nanowires is presented in Fig. 1(b). These figures confirm that no photoresist or other contaminants remain on the nanowire surfaces. This indicates that the post-fabrication cleaning process was effective. Maintaining clean nanowire surfaces is essential for optimizing sensing performance, as any residual contaminants can degrade sensor sensitivity. As shown in Fig. 1, 20 nanowire strips were formed, each approximately 3 μm in length and 100 nm in width. By the sidewall spacer etching technique, nanowires were created on both sides of the dummy gate, resulting in two nanowire strips per dummy gate.

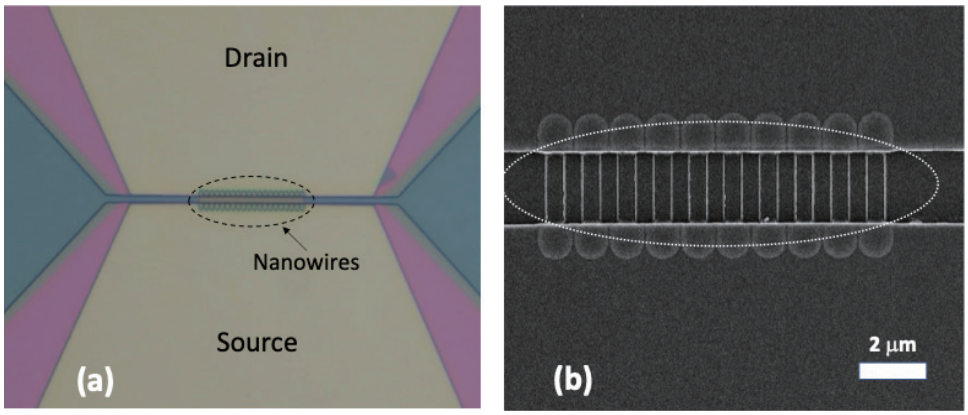

Fig. 1. (Color online) (a) Top-view optical microscopy image of poly-Si NWFET device. (b) SEM image of formed nanowires.

Figure 2 shows the electrical characteristics of the poly-Si NWFET biosensors measured in ambient air. Figure 2(a) shows the drain current (I_D) versus gate voltage (V_G) curve, recorded with a gate voltage sweep from −0.5 to 5 V and a constant drain voltage of 0.1 V. Each device is an n-channel, enhancement-mode transistor. The extracted threshold voltage (V_{TH}) is approximately 1.05 V, demonstrating that the drain current is predominantly controlled by the gate voltage. When the gate voltage is below 0 V, the drain current remains at 10^{-12} A. As V_G gradually increases but remains below V_{TH}, the drain current rises significantly. Once V_G exceeds V_{TH}, the drain current reaches 10^{-7} A, and the transistor enters the "ON" state.

Figure 2(b) shows the drain current versus drain voltage (I_D–V_D) characteristic curves. These curves were obtained with a drain voltage sweep from 0 to 2.5 V and a stepwise gate voltage increment of 0.5 V, ranging from 0 to 3 V. When a small V_D is applied, an electron channel forms in the nanowires, and I_D increases linearly with V_D. As V_D further increases, I_D reaches a constant value, indicating that the transistor has entered the saturation region. These characteristic curves provide insight into the switching behavior and overall performance of the nanowire FETs.

We then evaluated the biosensor's biological detection capabilities under various surface modifications and thermal treatments. The primary objective was to understand how these modifications affect the device's sensitivity and current response in detecting specific biomolecules. By correlating the effects of thermal treatments with biological detection results, we aimed to identify the optimal conditions that maximize sensor performance for biosensing applications.

Figure 3 shows the I_D–V_G curves of the poly-Si NWFET devices following various thermal treatments. These measurements were taken after functionalizing the devices with APTES and GA modifications. As shown, the curves exhibit significant shifts after both APTES and GA functionalizations, confirming the effectiveness of the modification process on the nanowire surfaces. Additionally, the variations in curve shifts under different thermal treatment conditions suggest that the surface modifications are affected by thermally induced chemical reactions on the nanowires.

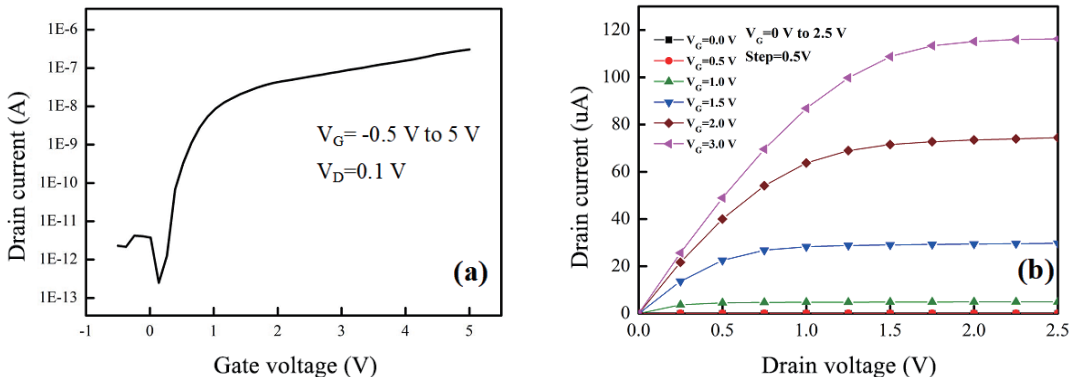

Fig. 2. (Color online) Electrical characteristics of poly-Si NWFET biosensors. (a) I_D–V_G and (b) I_D–V_D curves.

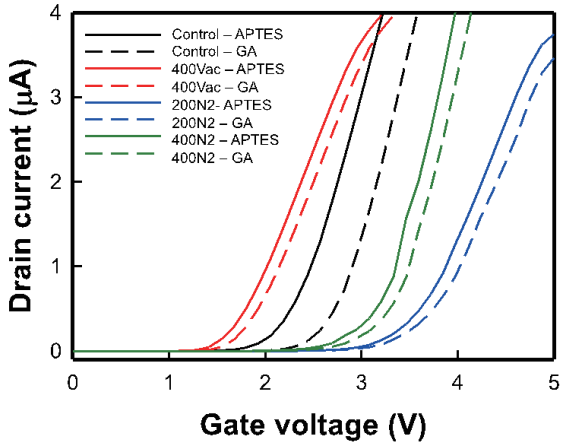

Fig. 3. (Color online) I_D–V_G curves of NWFET devices after surface functionalization and various thermal treatments.

To analyze the electrical characteristics of the poly-Si NWFET biosensors following various thermal treatments, key parameters such as subthreshold swing (*SS*), ON/OFF current ratio, and threshold voltage shift (ΔV_{TH}) were extracted from the I_D–V_G curves. Figure 4 shows the statistical *SS* results of the NWFET devices after treatments at 400 °C in vacuum, 200 °C in N_2, and 400 °C in N_2. For comparison, the as-deposited samples without any thermal treatment are also included in the figure. *SS* is a crucial parameter that reflects the transistor's gate control capability; a smaller *SS* value indicates higher switching speeds and lower leakage currents, which translates to reduced power consumption. Among the thermal treatments, the 400 °C vacuum treatment demonstrates a notable decrease in *SS* and more uniform results for the samples after APTES modification, as shown in Fig. 4(a). A similar trend is observed for the samples after GA modification, as depicted in Fig. 4(b).

The observed reduction in *SS* after the 400 °C vacuum thermal treatment can be attributed to several synergistic mechanisms that improve the electrostatic control of the gate over the poly-Si channel. *SS* is a critical indicator of how effectively the gate voltage modulates the channel

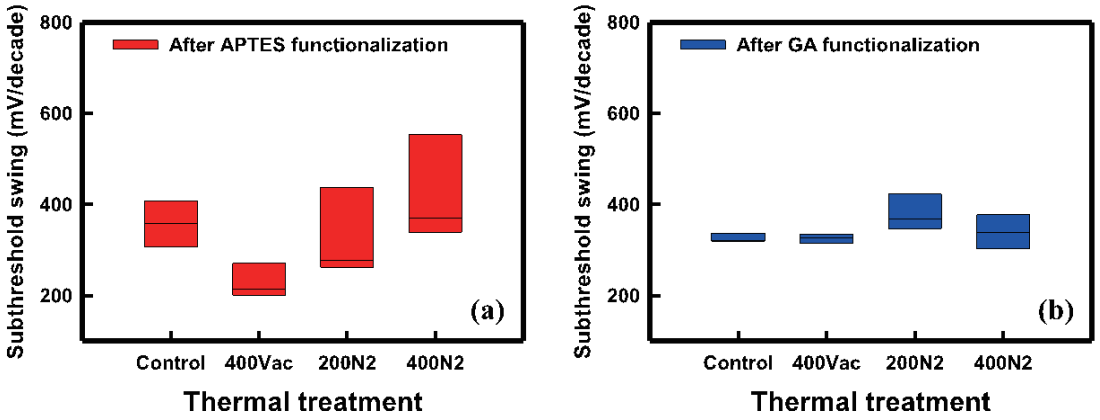

Fig. 4. (Color online) Statistical *SS* results of NWFET devices after different thermal treatments. (a) APTES and (b) GA functionalizations.

current, and it is strongly affected by the interface trap density and defect states in the channel and at the dielectric interface. In poly-Si NWFETs, grain boundaries and interface states—commonly arising from dangling bonds or residual contamination—introduce localized energy states that trap charge carriers, thereby degrading the gate control and resulting in a higher *SS*. Vacuum annealing at elevated temperatures has been reported to passivate these defect states, primarily by promoting the hydrogen desorption of volatile surface contaminants and allowing atomic rearrangement or recrystallization at the nanowire surfaces and grain boundaries. Specifically, the 400 °C vacuum environment is effective in reducing oxygen- and moisture-related surface states that are otherwise difficult to remove under ambient or nitrogen environments. Furthermore, vacuum annealing facilitates the partial healing of Si–Si bond defects and grain boundary reordering, thereby lowering trap densities both in the bulk poly-Si and at the Si/oxide interface. As a result, the density of trap-assisted tunneling and subthreshold leakage is significantly reduced, leading to a sharper subthreshold slope and improved switching characteristics.[14,15] The obtained results suggest that the 400 °C vacuum treatment optimally enhances the *SS* of the poly-Si NWFET devices, contributing to improved performance stability after surface modification.

Figure 5 shows the statistical ON/OFF current ratio results of the NWFET devices after various thermal treatments. The ON/OFF current ratio is a critical parameter for assessing transistor performance, as a high ratio indicates a strong drain current in the ON state and an ultralow leakage current in the OFF state. The poly-Si NWFET devices fabricated in this study achieved ON/OFF current ratios of up to five orders of magnitude. No significant difference in ON/OFF current ratio was observed across the different thermal treatments. The minimal variation in ON/OFF current ratio across different thermal treatment conditions, as presented on a logarithmic scale in Fig. 5, indicates that although thermal annealing significantly improves subthreshold characteristics and reduces interface trap densities, it does not markedly affect the fundamental carrier transport mechanisms or channel doping levels of the poly-Si nanowires, which predominantly govern the ON and OFF state currents.

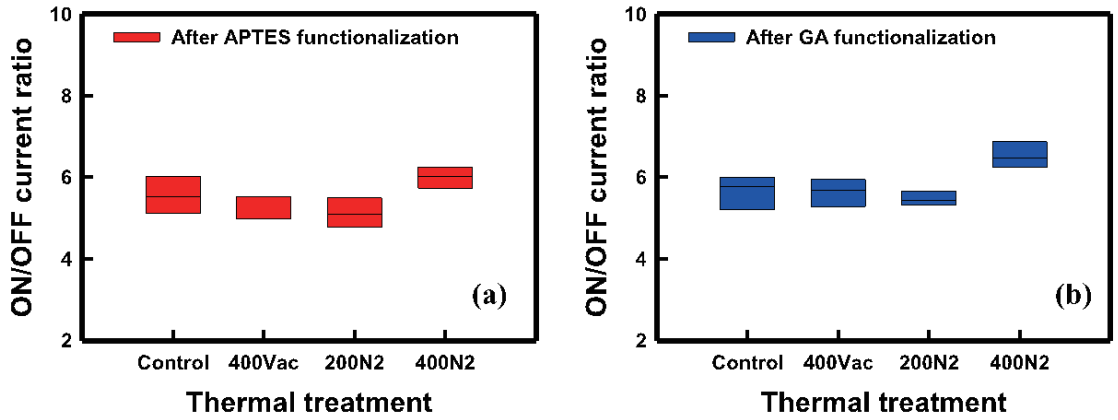

Fig. 5. (Color online) Statistical results of ON/OFF current ratio of NWFET devices after different thermal treatments. (a) APTES and (b) GA functionalizations.

The threshold voltage shift (ΔV_{TH}) is another important parameter for evaluating NWFET device performance. Figure 6 shows the statistical ΔV_{TH} results of the NWFET devices following each thermal treatment. The results indicate that 400N2 samples exhibit more stable ΔV_{TH} values than those subjected to other treatments. This suggests that the 400 °C N_2 treatment may provide optimal stability in threshold voltage behavior for the poly-Si NWFET devices. The observed trade-off between the improved ΔV_{TH} stability under 400 °C nitrogen annealing and the superior *SS* performance under 400 °C vacuum treatment may be attributed to the differing ambient effects during thermal processing. Nitrogen provides a relatively inert and passivating atmosphere, which helps stabilize the threshold voltage by mitigating the fixed oxide charge. In contrast, vacuum annealing is more effective at eliminating interfacial and grain boundary traps, thereby enhancing *SS* through improved gate-channel electrostatic coupling.

From the electrical characteristics presented in Figs. 4 to 6, the 400 °C vacuum treatment is preferable to the other methods for optimizing device performance. While the 400N2 sample exhibits a more stable ΔV_{TH}, the stability achieved with the 400Vac sample is also acceptable in terms of ΔV_{TH} and offers additional benefits in *SS* and ON/OFF current ratio. Thermal treatment plays a crucial role in enhancing the stability of our poly-Si NWFET device, given the material's inherent properties. By optimizing these thermal treatment parameters, along with the integration of microfluidic channels and a refined biosensing measurement technique, the sensitivity of the poly-Si NWFET biosensor can be significantly enhanced, making it a robust platform for biomedical applications.

To validate the biosensor's capability, solution pH sensing was performed using the 400Vac NWFET devices. Figure 7 shows the pH sensing results for the thermally treated poly-Si NWFET biosensor. The I_D–V_G curves for the biosensor in BTP buffer solutions with pH values ranging from 6 to 9 are shown in Fig. 7(a). The curves shift to the right as the solution pH increases from 6 to 9. This shift is expected, as the concentration of OH^- ions increases with pH. Surface functional groups on the nanowires, such as NH_3^+ and SiOH, interact with the increasing negative ion density, converting to NH_2 and SiO^-, respectively. These negative charges on the

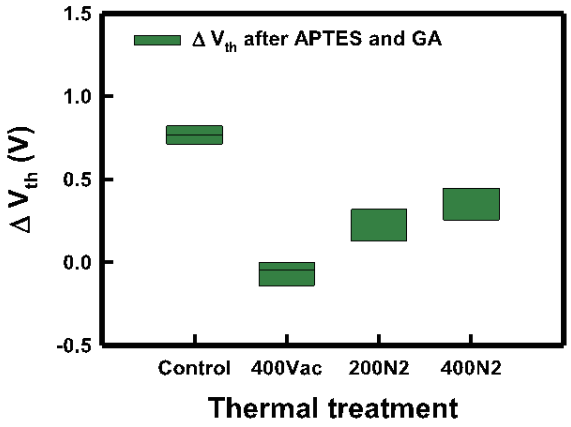

Fig. 6. (Color online) Statistical ΔV_{TH} results of NWFET devices after different thermal treatments. (a) APTES and (b) GA functionalizations.

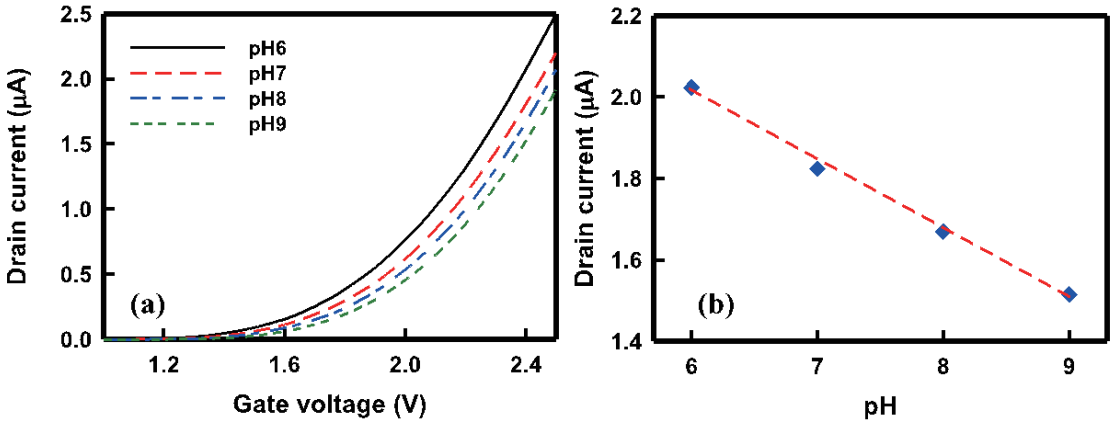

Fig. 7. (Color online) Solution pH sensing results of the poly-Si NWFET biosensor. (a) I_D–V_G curves of the solution pH from pH 6 to 9. (b) Drain current as a function of solution pH.

nanowire surfaces reduce the drain current, resulting in a rightward shift of the I_D–V_G curve. Figure 7(b) shows the calibration curve of the NWFET biosensor for pH sensing, where the drain current is measured at V_G = 2.4 V from the I_D–V_G curves. The data demonstrate a linear dependence of the drain current on the solution pH, confirming the device's effectiveness as a pH sensor.

Stability and response time are critical indicators for evaluating the performance of poly-Si NWFET biosensors. These characteristics were assessed through a real-time detection experiment. The experiment involved sequentially introducing buffer solutions of various pH values into the biosensors via a microfluidic channel and continuously monitoring the electrical response. Initially, a pH 6 buffer solution was injected, and the biosensors' drain current was symmetrically recorded. After approximately 1000 s—once the current reached equilibrium—the pH 6 solution was promptly expelled, and a pH 7 buffer solution was introduced while

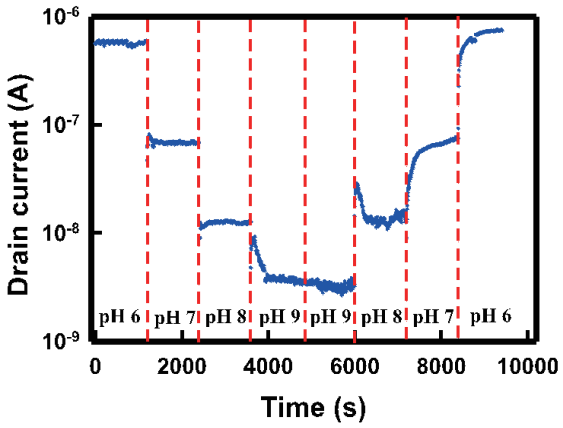

Fig. 8. (Color online) Real-time sensing result of poly-Si NWFET biosensor in detecting different pH values of the buffer solution.

maintaining real-time current monitoring. This process was repeated for buffer solutions of pHs 8 and 9 in sequence.

The real-time response of the NWFET biosensor treated at 400 °C in vacuum is illustrated in Fig. 8. The biosensor exhibited a clear stepwise change in drain current corresponding to each pH, registering 6.2×10^{-7}, 7.0×10^{-8}, 1.2×10^{-8}, and 3.4×10^{-9} A for pHs 6, 7, 8, and 9, respectively. When the buffer solution was switched back from pH 9 to pH 6, the drain current nearly returned to its original level, indicating excellent signal reversibility. These results confirm the biosensors' high stability and reliability in real-time pH sensing applications. In addition, nonlinearity and recovery hysteresis are observed in this figure. This result is attributable to the fact that real-time pH sensing may result from transient surface charge dynamics during the switching period, such as the incomplete desorption of ions or the slow re-equilibration of surface functional groups (e.g., NH_3^+/NH_2 and $SiOH/SiO^-$), which can cause delayed response and partial memory effects. This issue can be mitigated in future work by optimizing the surface functionalization chemistry and flow dynamics to enhance ion exchange efficiency and response uniformity.

4. Conclusions

We successfully fabricated poly-Si nanowires by a sidewall spacer technique and developed NWFET devices to function as biomedical sensors. The impact of thermal treatments on the electrical characteristics of poly-Si NWFET biosensors was systematically evaluated. The devices treated at 400 °C in vacuum demonstrated a *SS* swing, a stable threshold voltage shift, and an acceptable ON/OFF current ratio. These NWFET biosensors were then used to sense solution pH, displaying a linear dependence on pH. Real-time sensing results also demonstrated the excellent stability and reliability of the NWFET biosensors. The advancement of semiconductor-based biosensors promises to revolutionize medical diagnostics by enhancing biomarker detection, enabling early diagnosis, and facilitating personalized healthcare. This

interdisciplinary approach will play a pivotal role in improving the effectiveness and accessibility of medical diagnostic tools.

References

1 S. H. Lee, S. M. Lee, S. H. Chang, D. S. Shin, W. W. Cho, E. A. Kwak, S. M. Lee, and W. J. Chung: Biosens. Bioelectron. **273** (2025) 117156. http://doi.org/10.1016/j.bios.2025.117156
2 X. J. Zhang, L. S. Wong, Z. Y. Tang, H. M. Xiong, J. Y. Sun, L. B. Kong, M. Tu, Y. J. Hu, Y. Zhou, W. W. Zhu, K. J. Hsia, H. Wan, and P. Wang: ACS Sens. **10** (2025) 2994. http://doi.org/10.1021/acssensors.5c00021
3 N. Hamano and Y. Negishi: Sens. Mater. **34** (2022) 961. https://doi.org/10.18494/SAM3611
4 Y. Y. Chen, Z. M. Li, S. He, H. T. Lian, G. M. Liu, B. Liu, and X. F. Wei: Sens. Actua. B-Chem. **427** (2025) 137185. https://doi.org/10.1016/j.snb.2024.137185
5 M. A. Koussa, M. Barreiros, P. S. E. Perez, S. R. Jean, T. C. Lee, R. MacLeod, A. Witham, G. Bhat, T. Campbell, S. Lizano, M. Toth, A. Venkateswaran, D. Yang, N. Zaman, W. Alfaqheri, A. Ardalan, L. Barbosa, M. Behrouzi, V. Borisenko, R. Chand, K. S. Ho, P. Kumar, M. Lengyel, W. Luo, F. Masum, L. Piñeros, A. R. Kozhipuram, S. Sanders, D. Santos, V. Nadella, F. Kazemzadeh, and I. Khodadad: Sens. Diagn. **3** (2024) 1899. http://doi.org/10.1039/d4sd00105b
6 A. C. Poirier, R. D. R. Moreno, L. Takaindisa, J. Carpenter, J. W. Mehat, A. Haddon, M. A. Rohaim, C. Williams, P. Burkhart, C. Conlon, M. Wilson, M. Mcclumpha, A. Stedman, G. Cordoni, M. Branavan, M. Tharmakulasingam, N. S. Chaudhry, N. Locker, A. Fernando, W. Balachandran, M. Bullen, N. Collins, D. Rimer, D. L. Horton, M. Munir, and R. M. La Ragione: Front. Mol. Biosci. **10** (2023) 1. http://doi.org/10.3389/fmolb.2023.1144001
7 N. S. Lynn Jr., M. Forinová, M. Spasovová, H. Vaisocherová-Lísalová, and P. Yudin: Sens. Actua. B-Chem. **401** (2024) 134949. http://doi.org/10.1016/j.snb.2023.134949
8 C. H. Liu, J. J. Huang, R. X. Liu, Y. Zhu, and T. L. Xu: Sens. Actua. B-Chem. **437** (2025) 137759. http://doi.org/10.1016/j.snb.2025.137759
9 K. Kaewpradub, K. Veenuttranon, H. Jantapaso, P. Mittraparp-arthorn, and I. Jeerapan: Nano-Micro Lett. **17** (2025) 71. http://doi.org/10.1007/s40820-024-01561-8
10 Y. B. Manga, F.-H. Ko, Y.-S. Yang, J.-Y. Hung, W.-L. Yang, H.-M. Huang, and C.-C. Wu: Sens. Actua. B-Chem. **256** (2018) 1114. http://doi.org/10.1016/j.snb.2017.10.007
11 C. C. Wu: Biosensors **12** (2022) 115. http://doi.org/10.3390/bios12020115
12 S. S. Nemati, G. Dehghan, N. Sheibani, and Y. Abdi: IEEE Sens. J. **24** (2024) 17324. http://doi.org/10.1109/Jsen.2024.3389680
13 X. R. Yang, J. H. Du, H. S. Chen, C. J. Cui, H. B. Liu, and X. C. Zhang: Sens. Rev. **44** (2024) 525. http://doi.org/10.1108/Sr-03-2024-0184
14 C.-C. Wu and M.-R. Wang: Sens. **21** (2021) 4904. https://doi.org/10.3390/s21144904
15 M. G. Yirak and R. Chaujar: Adv. Cond. Matter. Phy. **2025** (2025) 1. https://doi.org/10.1155/acmp/3744806
16 C. H. Lee, W. P. Hu, and W. Y. Chen: Biosens. Bioelectron. **268** (2025) 116909. http://doi.org/10.1016/j.bios.2024.116909
17 C. C. Wu: J. Electrochem. Soc. **169** (2022) 077514. http://doi.org/10.1149/1945-7111/ac80d6